ACS APPLIED ENERGY MATERIALS

www.acsaem.org Article

Epitaxial CdTe Thin Films on Mica by Vapor Transport Deposition for Flexible Solar Cells

Xixing Wen,* Zonghuan Lu, Xin Sun, Yu Xiang, Zhizhong Chen, Jian Shi, Ishwara Bhat, Gwo-Ching Wang, Morris Washington, and Toh-Ming Lu

Cite This: *ACS Appl. Energy Mater.* 2020, 3, 4589–4599 Read Online

ACCESS | Metrics & More | Article Recommendations | Supporting Information

ABSTRACT: Most high-quality CdTe thin films are epitaxially grown on single-crystalline substrates through chemical bondings by either molecular beam epitaxy or metalorganic chemical vapor deposition. The epitaxial CdTe films are rarely applied in electronic or optoelectronic devices because of the rigid single-crystalline substrate. We present high-quality CdTe films epitaxially grown on mica by vapor transport deposition process through weak interface interactions. The full width at half-maximum (fwhm) of the X-ray diffraction rocking curve of CdTe (111) and the fwhm of azimuthal in-plane angular dispersion of CdTe (111) were 0.23° and 0.36°, respectively. The weak interaction at the interface enables a transfer of the epitaxial film from mica onto other flexible substrates for applications. The epitaxial CdTe film was separated from the mica substrate by the surface tension of water during immersion and then transferred onto a flexible SU-8 photoresist substrate for the fabrication of CdTe solar cells. We successfully fabricated the flexible all-epitaxial, epi-CdS/epi-CdTe solar cells with a power conversion efficiency of 9.59%, which showed low interface defects and high diode quality compared to the poly-CdS/epi-CdTe solar cells.

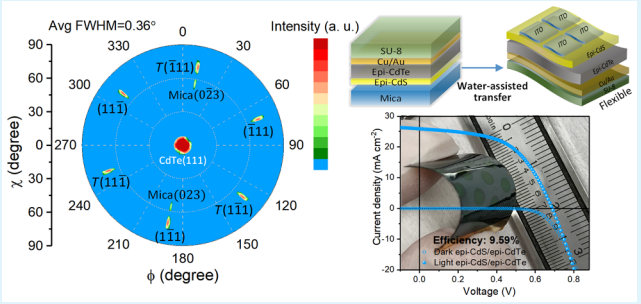

KEYWORDS: *CdTe, epitaxy, van der Waals, vapor transport deposition, flexible photovoltaics*

1. INTRODUCTION

Cadmium telluride (CdTe) is a widely used semiconductor material in the optoelectronic field.[1] Polycrystalline CdTe films have been used in commercial solar cell products.[2] So far, the efficiency of rigid CdTe solar cells has been improved to over 22%.[3] The rigid CdTe solar cells are fabricated on several millimeter thick glass substrates, while the solar cell stacks are only a few micrometers. The thick glass substrate takes up most of the total weight. Therefore, if the thick glass substrate can be substituted with a lightweight substrate, the specific power (ratio of the output power to the weight) of the solar cells will be improved. The specific power is an important parameter for the application of solar cells, such as consumer electronics, transportation, military, and space applications. One approach to improve the specific power is to use lightweight flexible or thin substrates. A record efficiency of 16.4% for the flexible CdTe solar cells has been reported, which was fabricated on a flexible willow glass substrate.[4,5] The efficiencies of flexible CdTe solar cells on polymer and metal foil substrates are reported to be 13.8% and 13.6%, respectively.[1,6] Comparing to the rigid CdTe solar cell efficiency, there is definitely room for the improvement of flexible CdTe solar cells. One of the approaches to improve the performance of solar cells is to increase the carrier lifetime through improving the film quality.[7,8] Long carrier lifetime and low recombination are prerequisite for high efficiency.[8] This approach has been employed in rigid CdTe solar cells. With the epitaxial monocrystalline CdTe absorber, the high open-circuit voltage over 1 V was achieved, and the corresponding efficiency was 17%.[7] However, the high-quality epitaxial CdTe film is rarely studied for flexible solar cells due to the restriction of the single-crystalline substrate.

Often, high-quality CdTe films are heteroepitaxially grown on rigid single-crystalline substrates with a close lattice matching through chemical bondings. This stringent requirement restricts the application of epitaxial CdTe films. Recently, there has been considerable interest in growing epitaxial films through weak interface interactions such as van der Waals (vdW) interaction. van der Waals epitaxy (vdWE) is a heteroepitaxy growth technique that relaxes the lattice matching requirement between an epitaxial film and a single-crystalline substrate.[9] It is based on the weak intermolecular force among atoms at the interface of the epitaxial film and the

Received: February 7, 2020
Accepted: April 14, 2020
Published: April 14, 2020

https://dx.doi.org/10.1021/acsaem.0c00265
ACS Appl. Energy Mater. 2020, 3, 4589–4599

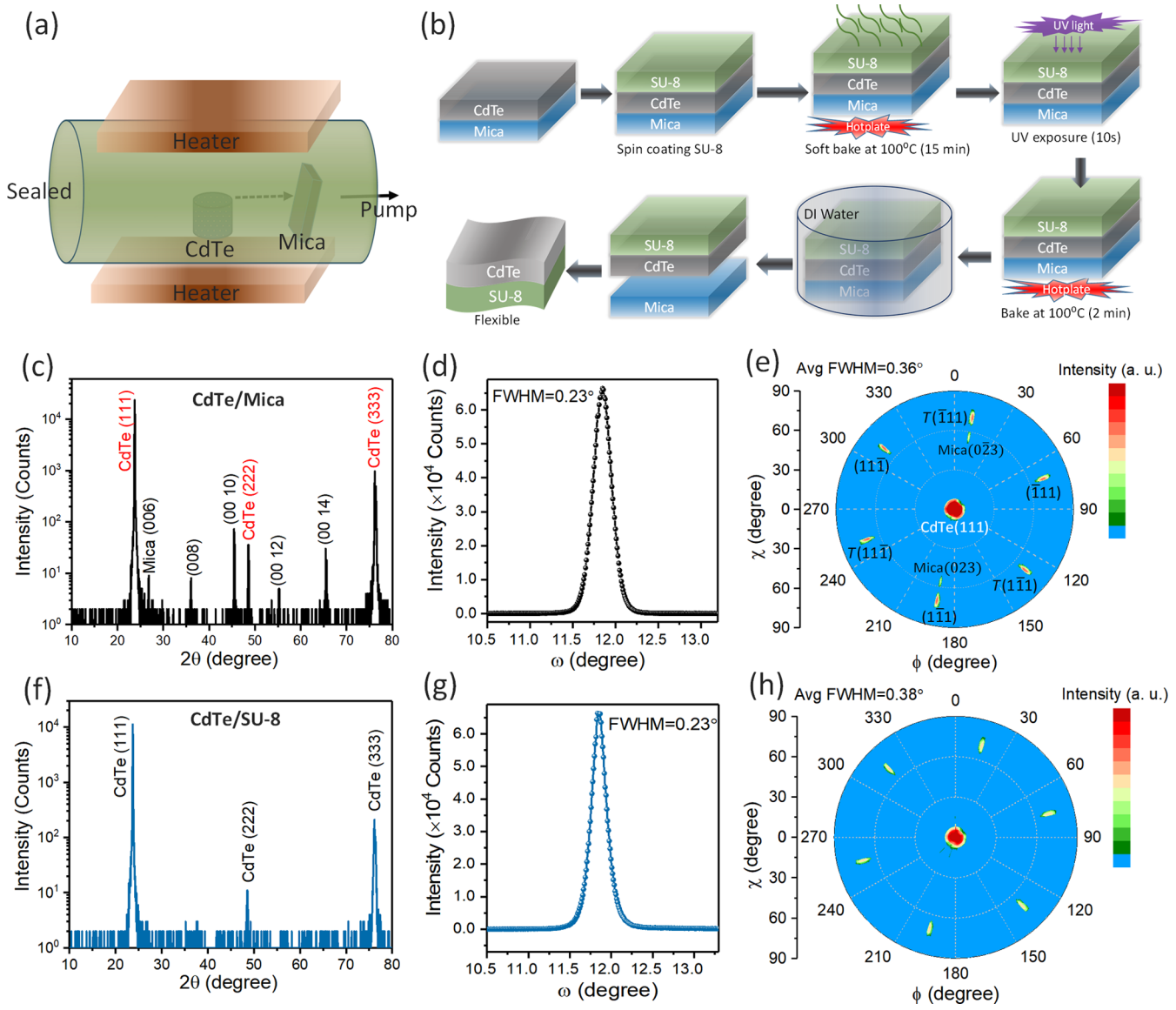

Figure 1. (a) Schematic diagram of a VTD system. (b) Schematic illustrations of the transfer process for epi-CdTe films from mica. (c) XRD θ–2θ scan, (d) XRD rocking curve of the CdTe (111), and (e) XRD CdTe {111} pole figure at $2\theta = 23.7°$, of the epi-CdTe film on mica grown at T_{source} of 600 °C, T_{sub} of 420 °C, and P of 4 mTorr. (f) XRD θ-2θ scan, (g) XRD rocking curve of the CdTe (111), and (h) XRD CdTe {111} pole figure of the transferred epi-CdTe film on SU-8 substrate.

vdW substrate. Due to the lack of "dangling bond" at the vdW surface, the requirement of lattice matching in a conventional chemical (bonding) epitaxy can be relaxed.[10] Furthermore, the vdW interface enables the transferring of an epitaxial CdTe film from a vdW substrate to another arbitrary substrate, thus suggesting great potential applications in flexible solar cells and other optoelectronic devices. Muscovite mica ($K_2O{\cdot}Al_2O_3{\cdot}SiO_2$), a layered material, has been traditionally considered to be a vdW type of material with a weak surface interaction.[10] However, recent experiments and density functional theory calculations indicated that when a 3D material is deposited on the mica surface, there may also exist a chemical interaction component that involves an exchange of charges in addition to the traditional vdW forces.[10,11] The interaction between the epitaxial film and the mica substrate is therefore somewhat stronger than a traditional vdW surface but weaker than a purely chemical nature. Nevertheless, it is still sufficiently weak so that the epitaxial film can be detached from the substrate surface. Also, mica is flexible, thermally stable (up to 700 °C), durable, commercially available, low cost, atomically flat, and chemically inert and can be easily cleaved from bulk mica.[10,12] It has been widely used as a template for vdW epitaxy.[9,10,12−14] All of these attributes can greatly facilitate the application of epitaxial CdTe films.

The diverse growth techniques for the epitaxial CdTe films include molecular beam epitaxy (MBE),[12] metalorganic chemical vapor deposition (MOCVD),[10,15] pulse laser deposition (PLD),[16] hot wall epitaxy,[17] close space sublimation (CSS),[18] and vapor transport deposition (VTD).[19,20] MBE and MOCVD have been attempted for vdW epitaxy of CdTe films on mica.[10,12] However, their growth rates are rather slow, about 4 nm/min for MBE and 1.7 nm/min for MOCVD, and thus increase the cost of CdTe films. Among these techniques, VTD is a high-rate, low-cost scalable manufacturing technique.[21] It has a great potential for epitaxial growth of CdTe films. Ultrathin CdTe nanosheets have been

https://dx.doi.org/10.1021/acsaem.0c00265
ACS Appl. Energy Mater. 2020, 3, 4589−4599

grown on mica substrates using the VTD method.[14] However, the epitaxial CdTe film grown on mica by VTD has not been reported thus far.

In the present work, we demonstrate the epitaxial growth of CdTe films on mica substrates using the VTD process. Mica substrate is not conductive, and an epitaxial film on mica cannot be directly used for the vertical device fabrication. On the basis of the weak interaction between epitaxial CdTe film and mica substrate, we developed a water-assisted transfer process for transferring of the epitaxial CdTe film from mica onto another substrate of interest for solar cell fabrication. In this process, it is particularly attractive that the ability to reuse the mica substrate allows savings on the cost of substrates. Herein, the SU-8 photoresist was spin-coated on the CdTe film as a flexible support substrate for the transfer of CdTe film. Immersion in deionized (DI) water was used to enable the separation of the CdTe film from the mica substrate. X-ray diffraction (XRD), electron backscattering diffraction (EBSD) crystallographic orientation mappings, and pole figures were performed to characterize the as-grown and the transferred CdTe films. The results show that the CdTe films grown on mica substrates by VTD process are [111]-orientated single-crystalline films. The high quality of the CdTe film is revealed by the full width at half-maximum (fwhm) of the CdTe (111) rocking curve and the fwhm of in-plane angular dispersion values of 0.23° and 0.36°, respectively. Furthermore, the scanning electron microscope (SEM) and atomic force microscope (AFM) images reveal no cracks and damages in the transferred CdTe films. Meanwhile, we fabricated flexible CdTe solar cells using the transferred epitaxial films and obtained indium tin oxide (ITO)/epi-CdS/epi-CdTe/Cu/Au/SU-8 flexible solar cells with a power conversion efficiency (PCE) of 9.59%.

2. EXPERIMENTAL SECTION

2.1. Growth and Transfer of CdTe Thin Films. The CdTe thin films were grown on mica substrates by a VTD process using CdTe polycrystalline powder (Sigma-Aldrich, 99.98% purity) as the precursor. A schematic diagram of VTD system is shown in Figure 1a. CdTe (0.4 g) powder was put into a crucible and placed in the center of a VTD system (a single temperature zone quartz tube furnace). A freshly cleaved mica substrate was placed and tilted (about 60°) at the right end of the heater in the VTD system. The source temperature (T_{source}) was controlled by the heater, and the substrate temperature (T_{sub}) was adjusted through varying the distance between the substrate and the heating center, and monitored by a type K thermocouple. The vacuum was maintained by a mechanical pump, and a stabilized chamber pressure (P) of 4 mTorr was controlled by changing the ventilation power of the pump. Before heating the powder source, the chamber was purged by flowing argon (Ar) gas with a flow rate of 200 sccm. During the growth of CdTe films, the Ar gas was turned off. The heating temperature was raised to the targeted temperature with a ramp rate of 15 °C/min and maintained for 10 min to grow a desired CdTe film. Then, the power of the VTD system was turned off to stop the growth, and finally the sample was taken out when the system naturally cooled to about 100 °C.

For the transfer of CdTe films from mica substrates, the schematic steps are depicted in Figure 1b. After the growth of CdTe film on mica, a SU-8 photoresist (Microchem, SU-8 3050) layer with a thickness of 70 μm was spin-coated on the CdTe surface as a flexible support substrate at 2000 rpm for 1 min. The SU-8/CdTe/mica stacks were subsequently soft baked on a hot plate at 100 °C for 15 min, cured under ultraviolet (UV) light for 10 s, and baked again for the strengthening of SU-8 on a hot plate at 100 °C for 2 min. Following that, the SU-8/CdTe/mica stack was immersed in DI water for the separation of SU-8/CdTe from mica substrate. Owing to the weak interaction, water molecules diffused into the weak interface between CdTe and mica. After about 5−10 s, the surface tension of water separated the SU-8/CdTe stack from the mica substrate. The whole (wafer-scale) CdTe film was thus transferred to the flexible SU-8 substrate. The mica substrate is reusable for the growth of CdTe films.

2.2. Device Fabrication. We fabricated flexible CdTe solar cells using two methods. One was depositing a polycrystalline CdS buffer layer on the transferred epi-CdTe film to build the device, which was defined as a poly-CdS/epi-CdTe device. The other one was depositing epi-CdTe film on the epi-CdS buffered mica substrate and transferring the epi-CdTe/epi-CdS stack for the device fabrications, defined as a epi-CdS/epi-CdTe device. A epi-CdS buffer layer with a thickness of 100 nm was deposited on the freshly cleaved mica by a thermal evaporation method. During the deposition, the substrate was not intentionally heated. CdS polycrystalline pieces (Alfa Aesar, 99.999% purity) were used as the evaporation source. The deposition rate and film thickness were monitored by a quartz crystal microbalance. The epi-CdS/mica was annealed on a hot plate at 400 °C for 6 min in ambient air. Then, 2.5 μm thick epi-CdTe films were deposited on both freshly cleaved mica and epi-CdS/mica substrates. After that, the epi-CdTe/mica and epi-CdTe/epi-CdS/mica samples were annealed in $CdCl_2$ (Sigma-Aldrich, 99.99% purity) vapor at 390 °C for 20 min using a horizontal furnace. Here, it should be noted that the $CdCl_2$ treatment cannot be performed using $CdCl_2$ solution, and any solution will separate the film from mica substrate due to the weak interaction at the interface. Subsequently, a Cu(2.5 nm)/Au(100 nm) bilayer was thermally evaporated on epi-CdTe/mica and epi-CdTe/epi-CdS/mica as the back-contact. The stacks were annealed in nitrogen atmosphere at 200 °C for 20 min to improve the back-contact. Following that, epi-CdTe/Cu/Au and epi-CdS/epi-CdTe/Cu/Au stacks were transferred onto the SU-8 flexible substrates using the transfer method shown in Figure 1b. Meanwhile, a polycrystalline CdS buffer layer (100 nm) was deposited by thermal evaporation on the epi-CdTe/Cu/Au/SU-8 stack at room temperature. Finally, a 220 nm ITO (In_2O_3:Sn) layer was sputtered on the two kinds of CdS/CdTe/Cu/Au/SU-8 samples as the front contact through a shadow mask for a device area of 0.049 cm^2.

2.3. Film and Device Characterizations. XRD data were collected by a Bruker D8 Discover X-ray diffractometer (Cu Kα, λ = 1.5406 Å). The step sizes of 0.02°, 0.01°, and 2° were used for the XRD $\theta-2\theta$ scan, rocking curve scan, and the pole figure scan, respectively. For the azimuthal (ϕ) scans at a fixed χ angle, a step size of 0.1° was used. SEM images were taken by a Zeiss Supra 55 SEM using an electron beam energy of 1.5 keV. AFM characterization was carried out using an AFM (PSI XE100) in the noncontact mode. EBSD measurement was performed by a Carl Zeiss Ultra 1540EsB SEM-FIB system integrated with a NordlysNano EBSD detector (Oxford Instruments). The current density−voltage ($J-V$) curves of the devices were acquired by a Keithley 2400 source meter under dark and simulated AM 1.5G (100 mW cm^{-2}) illumination generated by a xenon light source (Oriel, Model 9119, Newport) in ambient air at room temperature. The external quantum efficiency (EQE) of the solar cells was measured using a light source generated by a xenon lamp of Newport (Oriel, 6911). Then the light was split into specific wavelengths by a Newport Oriel Cornerstone 130 1/8 Monochromator (Oriel, model 74004). A standard silicon detector (70356_70316NS_302) was used for the calibration. The capacitance−voltage ($C-V$) profiling and deep-level capacitance profiling (DLCP) data were collected using Keithley 4200 semiconductor characterization system. $C-V$ measurements were carried out at room temperature in an electromagnetic shielding box at a frequency of 10 kHz and AC amplitude of 30 mV. The DC bias voltage was scanned from −1.5 to 0.5 V. DLCP measurements were performed with an AC amplitude scanned from 10 to 140 mV at different bias voltage ranging from −0.2 to 0.2 V. Photoluminescence (PL) measurements were carried out with a customized system consisting of a Picoquant 405 nm pulsed laser (2 mW), a microscope, a Princeton Instruments SP-2358 spectrograph, and a Thorlabs 4 megapixel monochrome scientific CCD camera.

https://dx.doi.org/10.1021/acsaem.0c00265
ACS Appl. Energy Mater. 2020, 3, 4589−4599

3. RESULTS AND DISCUSSION

3.1. Characterization of the As-Grown epi-CdTe Thin Films on Mica and the Transferred epi-CdTe Thin Films on SU-8. The CdTe films were grown on mica substrates at different T_{source}, T_{sub}, and P to optimize the film quality. XRD measurements were performed to study the epi-CdTe thin films grown at different growth conditions. XRD $\theta-2\theta$ scan was used to examine the out-of-plane orientation of the CdTe films. The rocking curve and the pole figure or azimuthal scan were used to examine the film's out-of-plane quality and the in-plane epitaxial orientation, respectively. The CdTe film grown at the optimized growth condition (T_{source} of 600 °C, T_{sub} of 420 °C, and P of 4 mTorr) was selected as a typical representative to study the properties of epi-CdTe films grown on mica by the VTD process. Figure 1c shows the XRD $\theta-2\theta$ scan of a 3.4 μm CdTe film on mica grown at the optimized growth condition. The peaks at 2θ of 26.5°, 35.7°, 45.0°, 54.7°, and 64.8° are from the (006), (008), (00 10), (00 12), and (00 14) planes of the single-crystal mica (001),[10] respectively. Meanwhile, the (111), (222), and (333) peaks of CdTe film are observed at 2θ around 23.7°, 48.6°, and 76.3°, respectively. Figure 1d shows the CdTe (111) rocking curve of the optimized CdTe film on mica. The fwhm of the rocking curve is about 0.23°, which indicates the out-of-plane quality of the epitaxial films. To check the in-plane orientation and quality, the XRD CdTe {111} pole figure (at 2θ = 23.7°) of the CdTe film grown at optimized condition is depicted in Figure 1e. Six poles with 60° apart in the azimuth direction at χ = 70.5° are observed. The average fwhm of the six poles in the azimuthal direction is about 0.36°. Theoretically, the CdTe {111} pole figure should have three poles with 120° azimuth angle apart at χ = 70.5°. The observed six poles imply a second set of orientation grains exists in the film, which is the twin of the first set of primary orientation grains, as labeled in Figure 1e. Moreover, the mica (023) and ($0\bar{2}3$) poles at χ = 56.2° are observed in Figure 1e, which are parallel to the two of six CdTe {111} poles. It is consistent with the epi-CdTe films grown on mica by MOCVD.[10,15] The in-plane epitaxial relationships of CdTe (111) and mica (001) are CdTe [$\bar{1}2\bar{1}$]//mica [010] and CdTe [$10\bar{1}$]//mica [100]. For the optimization of epitaxial CdTe films by a VTD process, the XRD data of CdTe films grown at other conditions are given in Supporting Information Figure S1. Table 1 summarized the XRD results. All of the CdTe films have the [111] out-of-plane orientation. The smallest fwhm (0.23°) of CdTe (111) rocking curve was obtained at T_{source} of 600 °C, T_{sub} of 420 °C, and P of 4 mTorr, and the corresponding average fwhm of CdTe {111} poles in the azimuthal direction is about 0.36°, indicating the highest quality among all of these CdTe films.

Table 1. XRD Results of epi-CdTe Films on Mica Substrates Grown at Different Conditions by a VTD Process

T_{source} (°C)	T_{sub} (°C)	P (mTorr)	orientation	fwhm of (111) rocking curve (deg)	av fwhm of {111} azimuthal scan (deg)
600	380	4	[111]	0.32	0.40
600	420	4	[111]	0.23	0.36
600	450	4	[111]	0.38	0.48
580	420	4	[111]	0.37	0.56
620	420	4	[111]	0.28	0.42
600	420	10	[111]	0.42	0.55

The fwhms of CdTe (111) rocking curve (0.23°) and CdTe {111} poles (0.36°) for our optimized epitaxial CdTe film on mica are comparable with those (0.11° and 0.38°) of the CdTe films grown by MOCVD.[10] These values are much smaller than those (0.73° and 10.3°) of epitaxial CdTe films grown on graphene by MOCVD.[15] These results demonstrate that the highly orientated single-crystalline CdTe (111) films can be grown on mica substrates through a VTD process.

Figure 1f shows the XRD $\theta-2\theta$ scan of the transferred CdTe film on flexible SU-8 substrate, where the CdTe film was grown on mica at the optimized condition. Only CdTe (111), (222), and (333) peaks are observed in the XRD scan. The rocking curve of CdTe (111) is shown in Figure 1g. The fwhm of the rocking curve is about 0.23°, which is the same as that of CdTe film on mica before its transfer (Figure 1d). The XRD CdTe {111} pole figure of CdTe/SU-8 is depicted in Figure 1h. There are also six poles observed at χ = 70.5° in the pole figure. The average fwhm of these poles in the azimuthal direction is about 0.38°, almost the same as that (0.36°) of CdTe film on mica substrate before transfer (Figure 1e). This result indicates the crystal quality of CdTe films was preserved and no damages occurred during the transfer process.

Panels a and b of Figure 2 show the SEM and AFM (20 μm × 20 μm) images of the epi-CdTe film on mica, respectively. The surface morphology of the epi-CdTe film shows a predominantly triangular shaped pyramidal, consistent with the (111) face of CdTe. The vertical root-mean-square (RMS) roughness extracted from the AFM image (Figure 2b) is about 207 nm. Panels c and d of Figure 2 are SEM and AFM (20 μm × 20 μm) images of the surface of the post-transferred epi-CdTe film on SU-8 substrate, respectively. As shown in Figure 2c, the surface of the transferred epi-CdTe film is very flat and smooth and no mica layers are observed on the surface. The vertical RMS roughness of the surface of the transferred epi-CdTe film extracted from Figure 2d is about 3.6 nm. This is attributed to the chemical inertness and atomically smooth surface of the mica (001) face. We can obviously observe many triangular convex and diamond concave sites, as marked by dashed lines in Figure 2d. The shaped morphologies are typical features of the CdTe (111) face, in agreement with the intrinsic zinc-blende structure of CdTe. The sides of the triangles and diamonds are parallel to each other, implying the nucleation and growth of CdTe were along one direction on the surface of mica substrate. In addition, Raman spectra of the epi-CdTe film on mica and the transferred epi-CdTe film on SU-8 using 514 nm laser excitation are shown in Figure S2. The two spectra are almost identical. For both samples, E(Te), A_1(Te), E(Te)/TO(CdTe) and LO(CdTe) modes are observed. The E(Te) and A_1(Te) modes may arise from Te precipitates, and E(Te)/TO(CdTe) and LO(CdTe) modes originated from bulk CdTe crystals.[22,23] Meanwhile, there are no mica modes found in the spectrum of the transferred epi-CdTe film, further confirming no mica layers or flakes left on the rear surface of the transferred epi-CdTe film.

EBSD was performed on the epi-CdTe/mica and the transferred epi-CdTe/SU-8 samples to further study the microstructure of the epitaxial CdTe films. Figure 3a shows the crystallographic orientation mapping of the epi-CdTe film on mica using the inverse pole figure (IPF)-Z component, which correlates the spatial crystallographic orientation with respect to the normal of the sample surface. The mapping shows a single blue color, suggesting a uniform [111] out-of-plane orientation across the whole scan area. It is consistent

https://dx.doi.org/10.1021/acsaem.0c00265
ACS Appl. Energy Mater. 2020, 3, 4589−4599

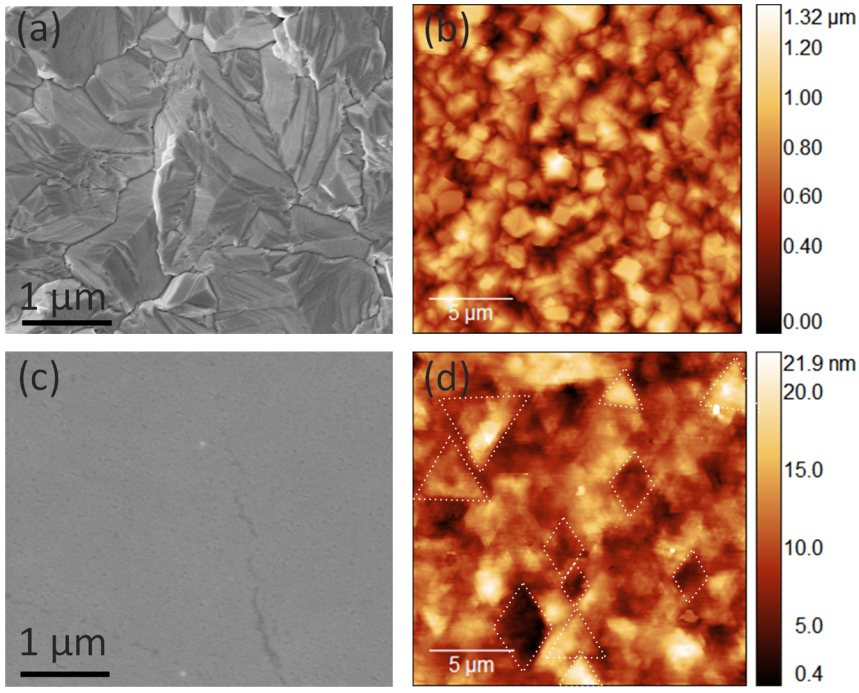

Figure 2. (a) SEM top-view and (b) AFM (20 μm × 20 μm) images of epi-CdTe film on mica substrate grown at T_{source} of 600 °C, T_{sub} of 420 °C, and P of 4 mTorr. (c) SEM and (d) AFM (20 μm × 20 μm) images of the surface of the transferred epi-CdTe film on SU-8 substrate.

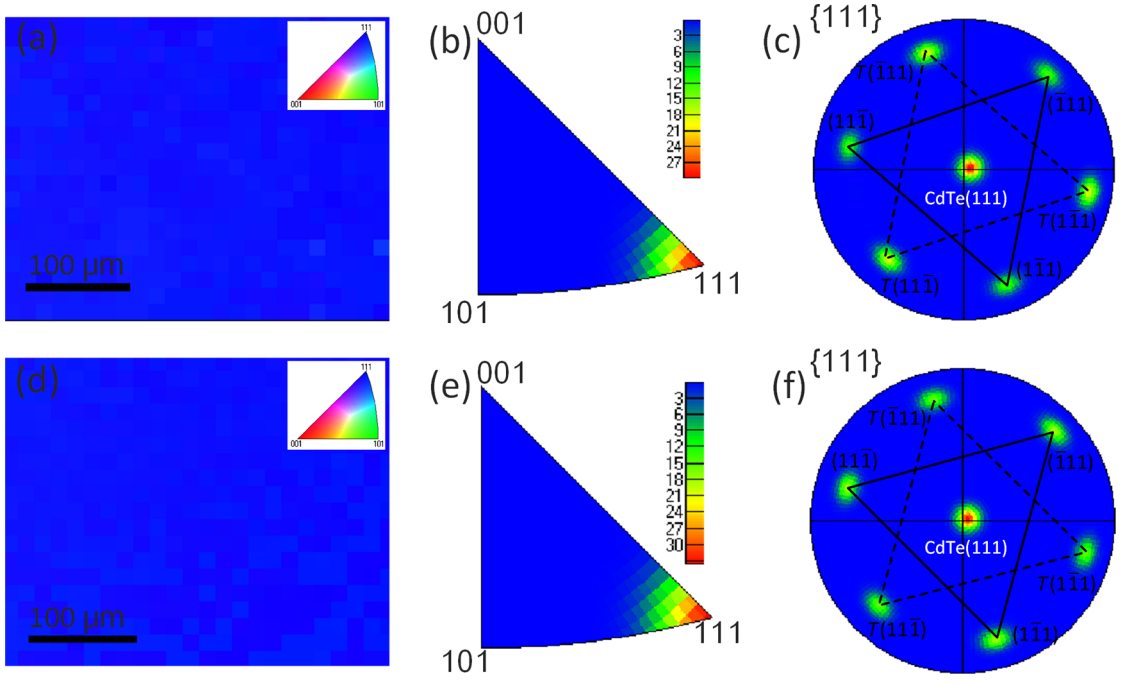

Figure 3. (a) EBSD crystallographic orientation mapping using IPF-Z component, (b) IPF-Z and (c) EBSD CdTe (111) pole figure of the CdTe film on mica. (d) EBSD crystallographic orientation mapping using IPF-Z component, (e) IPF-Z and (f) EBSD CdTe (111) pole figure of the transferred CdTe film on SU-8 substrate.

with the XRD result, shown in Figure 1c. The IPF-Z in Figure 3b further confirms the [111] out-of-plane orientation. Figure 3c shows the CdTe (111) EBSD pole figure of the scan area (Figure 3a). One can observe six poles separated by 60° relative to each other in the azimuthal direction, including three primary poles and three twin poles, as marked in Figure 3c. It further demonstrates the two sets of orientational grains in the epitaxial CdTe film on mica with a 60° rotation. Panels d–f of Figure 3 show the IPF-Z mapping, IPF-Z and CdTe (111) EBSD pole figure collected from the surface of the transferred CdTe film on SU-8 substrate, respectively. They are almost the same as the EBSD data from the CdTe film on mica. It can also be concluded that the transfer process does not change and degrade the quality of the epi-CdTe film.

3.2. Structure and Performance of Flexible Solar Cells with the Epitaxial CdTe Films. Figure 4a shows a schematic

https://dx.doi.org/10.1021/acsaem.0c00265
ACS Appl. Energy Mater. 2020, 3, 4589–4599

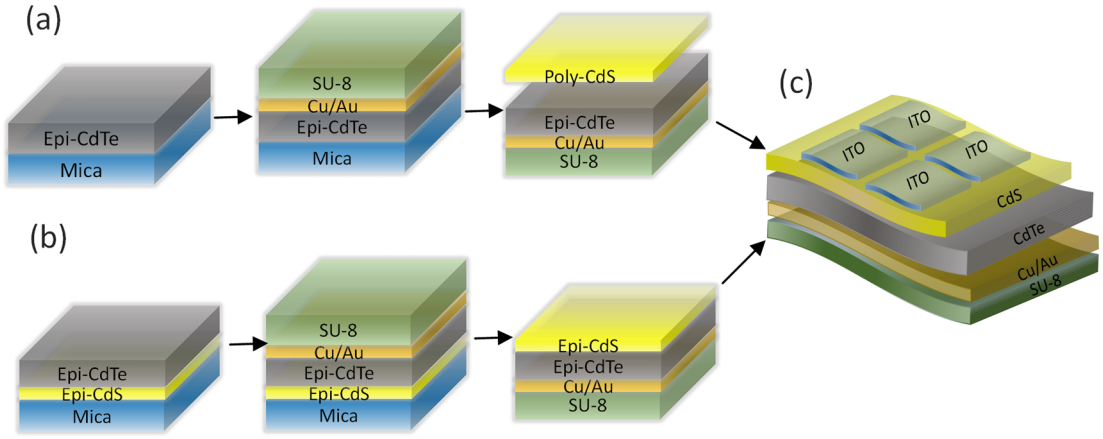

Figure 4. Schematic illustrations for the fabrication of (a) poly-CdS/epi-CdTe and (b) epi-CdS/epi-CdTe flexible solar cells. (c) Schematic architecture of the flexible CdTe solar cells.

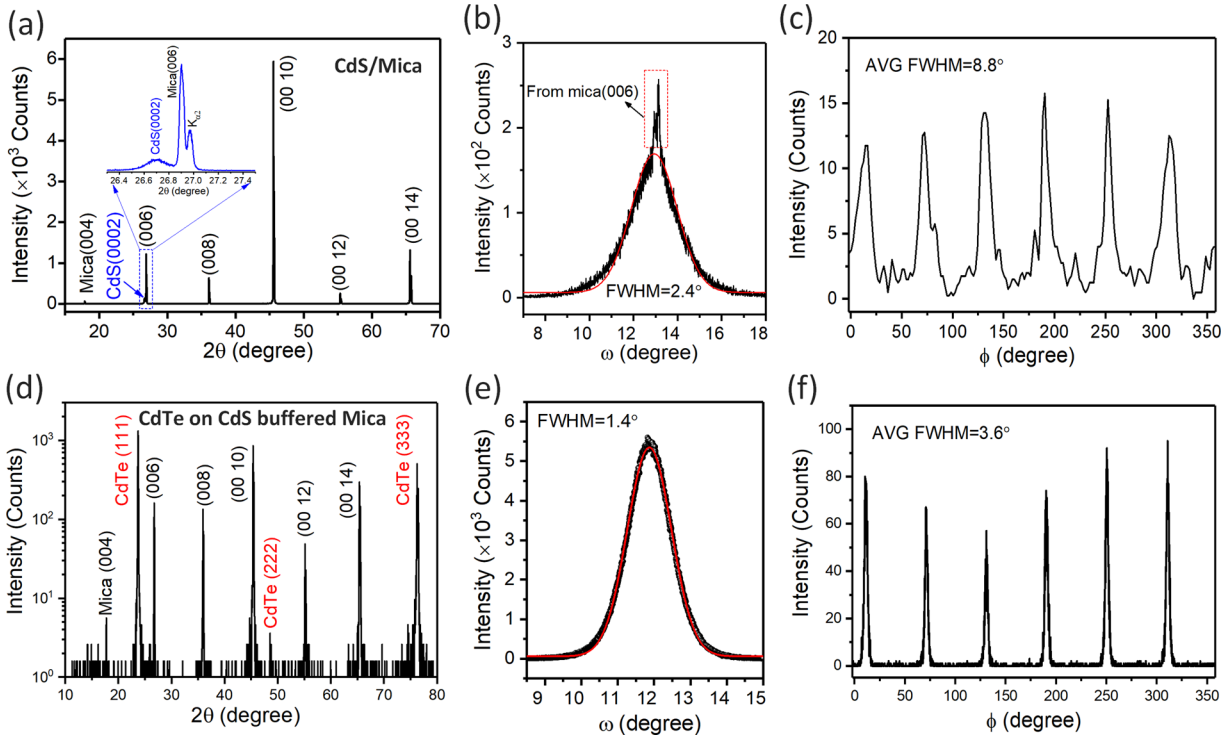

Figure 5. (a) XRD θ–2θ scan, (b) XRD rocking curve of the CdS(0002) diffraction, and (c) XRD CdS $\{10\bar{1}1\}$ azimuthal scan at $2\theta = 28.4°$ and $\chi = 62°$ of the epi-CdS buffer layer on mica. (d) XRD θ–2θ scan, (e) XRD rocking curve of the CdTe (111) diffraction, and (f) XRD CdTe $\{111\}$ azimuthal scan at $2\theta = 23.7°$ and $\chi = 70.5°$ of epi-CdTe on epi-CdS/mica substrate.

of the steps for the fabrication of flexible poly-CdS/epi-CdTe solar cells. The epi-CdTe film was grown on mica substrate and then transferred onto flexible SU-8 substrate. A poly-CdS layer was deposited on epi-CdTe/Cu/Au/SU-8 to build the poly-CdS/epi-CdTe device. Figure 4b describes the fabrication steps of the flexible solar cells with both epi-CdS buffer layer and epi-CdTe layer. As reported previously,[13] the CdS film could be epitaxially grown on the mica substrate followed by the epitaxial growth of the CdTe film on epi-CdS/mica by MOCVD. Therefore, to fabricate the flexible solar cells with all-epitaxial CdS/CdTe, the epi-CdS buffer layer was first grown on mica through thermal evaporation; then epi-CdTe film was deposited on epi-CdS/mica by VTD. The full fabrication details are described in Experimental Section. The final flexible device with a structure of ITO/CdS/epi-CdTe/Cu/Au/SU-8 is depicted in Figure 4c.

Furthermore, to check the film quality of the epi-CdS buffer layer deposited on the mica substrate and the epi-CdTe film on the epi-CdS/mica substrate mentioned in the second fabrication process (Figure 4b), XRD measurements were performed on these two films. Figure 5a shows the XRD θ–2θ spectrum of the epi-CdS buffer layer on the mica substrate. A small peak near the mica (006) peak was observed. This small peak is from CdS (0002).[13,24,25] The inset of Figure 5a is a magnified spectrum of the CdS (0002) and mica (006) peaks. The CdS (0002) peak is at about 26.68°. Figure 5b gives the rocking curve of the CdS (0002) peak. Because the CdS (0002) peak is very close to the mica (006) peak, a very sharp peak from mica (006) is also observed above the broad peak

https://dx.doi.org/10.1021/acsaem.0c00265
ACS Appl. Energy Mater. 2020, 3, 4589–4599

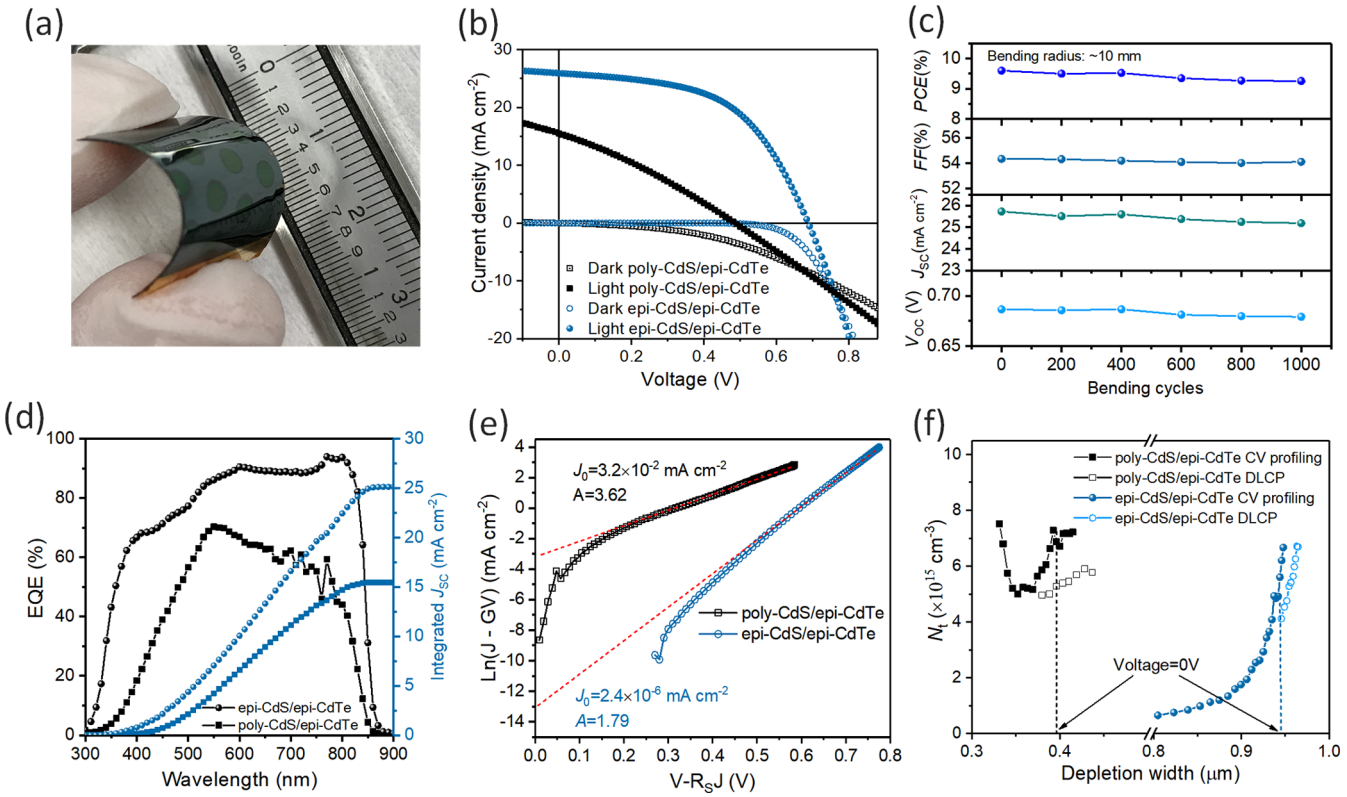

Figure 6. (a) Photograph of the flexible ITO/epi-CdS/epi-CdTe/Cu/Au/SU-8 solar cell. (b) Dark and light (under AM1.5 G illumination) $J-V$ curves of poly-CdS/epi-CdTe and epi-CdS/epi-CdTe devices. (c) Photovoltaic parameters of the epi-CdS/epi-CdTe device as a function of bending cycles under radius of curvature of 10 mm. (d) External quantum efficiency (EQE) and integrated J_{SC}, (e) plots of $\ln(J - GV)$ with respect to $V - R_SJ$ for the device parameters of J_0 and A, and (f) $C-V$ profiling and DLCP of the flexible poly-CdS/epi-CdTe and epi-CdS/epi-CdTe devices.

Table 2. Summary of Performance Parameters of the poly-CdS/epi-CdTe and the epi-CdS/epi-CdTe Devices[a]

device	PCE (%)	V_{OC} (V)	J_{SC} (mA cm^{-2})	FF (%)	Integrated J_{SC} (mA cm^{-2})	J_0(mA cm^{-2})	A	N_i (cm^{-2})
poly-CdS/epi-CdTe	2.22	0.485	15.5	29.6	15.4	3.2 × 10^{-2}	3.62	8.2 × 10^{10}
epi-CdS/epi-CdTe	9.59	0.687	25.7	54.3	25.2	2.4 × 10^{-6}	1.79	6.8 × 10^{10}

[a]The integrated J_{SC} is calculated by integrating the EQE spectra with standard AM1.5 spectrum. N_i is the interface defect density at CdS/CdTe interface, calculated from $C-V$ profiling and DLCP.

from CdS (0002) in the rocking curve, as marked by an open rectangle in Figure 5b. A fwhm of 2.4° was obtained from the fitting of the broad peak. Figure 5c shows the ϕ scan of CdS $\{10\bar{1}1\}$ at $2\theta = 28.4°$ and $\chi = 62°$. Six peaks with 60° azimuthal angular separation between adjacent peaks are found, which is consistent with the hexagonal symmetry of wurtzite CdS crystal structure.[13,25] The average fwhm of these six peaks is about 8.8°. Therefore, it can be concluded that the CdS buffer layer deposited on mica is an epitaxial single-crystalline film.

The XRD $\theta-2\theta$ spectrum, CdTe (111) rocking curve and azimuthal scan (at $\chi = 70.5°$) of the epi-CdTe film deposited on the epi-CdS/mica substrate are shown in Figure 5d–f, respectively. From the $\theta-2\theta$ spectrum, only the [111] orientation is observed in the epi-CdTe film on epi-CdS/mica. The fwhm of CdTe (111) rocking curve (Figure 5e) is about 1.4°, which is much smaller that of 2.6° from the epitaxial CdTe film grown on epi-CdS/mica by MOCVD.[13] For the in-plane orientation, there are also six peaks with 60° apart in the azimuthal scan of CdTe (111), as shown in Figure 5f. It is similar to the CdTe grown directly on mica (Figure 1e and Figure S1), with a second set of orientation domain. The average fwhm of these six peaks is about 3.6°, also smaller than that of 10.8° from the epi-CdTe film grown on epi-CdS/mica by MOCVD.[13] Therefore, we obtained epi-CdTe film on epi-CdS/mica substrate through a VTD process, and the quality is better than that grown by MOCVD.

The photograph of the flexible CdTe solar cells with a structure of ITO/epi-CdS/epi-CdTe/Cu/Au/SU-8 is shown in Figure 6a. In the photograph, the device was bent with a radius of 10 mm. The dark and light (under AM1.5 G illumination) current density–voltage (J-V) curves of poly-CdS/epi-CdTe and epi-CdS/epi-CdTe devices are shown in Figure 6b. The epi-CdS/epi-CdTe device shows a power conversion efficiency (PCE) of 9.59%, an open-circuit voltage (V_{OC}) of 0.687 V, a short-circuit current density (J_{SC}) of 25.7 mA cm^{-2}, and a fill factor (FF) of 54.3%, while the corresponding performance parameters of the poly-CdS/epi-CdTe device are 2.22%, 0.485 V, 15.5 mA cm^{-2}, and 29.6%, respectively. The performance parameters are summarized in Table 2. Obviously, the performance of the device with epi-CdS and epi-CdTe films is superior to that of the poly-CdS/epi-CdTe device. We examined the performance of the flexible epi-CdS/epi-CdTe solar cell with 1000 bending cycles. The photovoltaic parameters were recorded after every 200 bending

https://dx.doi.org/10.1021/acsaem.0c00265
ACS Appl. Energy Mater. 2020, 3, 4589–4599

cycles with about 10 mm bending radius, as exhibited in Figure 6c. The detailed $J-V$ curves and parameters are shown in Figure S3 and Table S1, respectively. The PCE, V_{OC}, J_{SC}, and FF decreased slightly with the increased bending cycles. The performance degradation was probably caused by the film stress. After 1000 bending cycles, the PCE was reduced from 9.59% to 9.25%. It indicates that excellent performance is maintained, with 96.5% of initial PCE retained after 1000 bending cycles with radius of curvature as small as 10 mm. This indicates a good bending property of the devices. Moreover, the normalized PCE of a flexible epi-CdS/epi-CdTe solar cell with initial 9.01% efficiency as a function of bending angle is exhibited in Figure S4. With the bending angle increasing from 0° to 58°, the PCE still retains 85.5% of its initial value. The flexible SU-8 photoresist substrate with a thickness of 70 μm is more flexible and lightweight than other flexible substrates, such as polyimide (PI) film and metal foil. The change in efficiency is attributed to the stress in the CdTe film.[26] The external quantum efficiencies of the two devices are given in Figure 6d. The photoresponse of the epi-CdS/epi-CdTe device is stronger than that of the poly-CdS/epi-CdTe device in all of the wavelength regions. This suggests the epi-CdS/epi-CdTe device possesses lower recombination losses of photogenerated carriers at the interface and in the whole absorb epi-CdTe layer.[27] The integrated J_{SC} with standard AM1.5 spectrum from the EQE spectra are 25.2 and 15.4 mA cm^{-2} for the epi-CdS/epi-CdTe and poly-CdS/epi-CdTe devices (summarized in Table 2), respectively, which almost agree with the J_{SC} values from the light $J-V$ curves of the two devices.

Generally, the device performance strongly depends on the reverse saturation current density (J_0) and diode ideality factor (A) of the photovoltaic device. To clarify why the epi-CdS/epi-CdTe device has a better performance than the poly-CdS/epi-CdTe device, the J_0 and A of the two devices were investigated by fitting the dark $J-V$ curves in Figure 6b.The $J-V$ behavior of the p−n junction can be expressed by a general single-exponential diode equation:[28−32]

$$J = J_0 \exp\left\{\frac{q}{AkT}(V - R_S J)\right\} + GV - J_L \quad (1)$$

where k is the Boltzmann constant, T is the temperature, q is the elementary charge, R_S is the series resistance, G is shunt conductance (dJ/dV), and J_L is the light current density. $J_L = 0$ under dark condition, and G can be obtained by taking the derivative of J with respect to V. Therefore, the relationship of J and V under dark condition can be expressed as

$$\ln(J - GV) = \frac{q}{AkT}(V - R_S J) + \ln J_0 \quad (2)$$

By transforming the dark $J-V$ curves to the plots of $\ln(J - GV)$ with respect to $V - R_S J$ (eq 2), as shown in Figure 6e, J_0 and A can be extracted from the intercept and the slope, respectively. The resulted J_0 and A of the poly-CdS/epi-CdTe device are 3.2 × 10^{-2} mA cm^{-2} and 3.62, respectively, while, for the epi-CdS/epi-CdTe device, J_0 and A are 2.4 × 10^{-6} mA cm^{-2} and 1.79, respectively, as shown in Table 2. It is known that the ideality factor (A) for a well-behaved solar cell is typically in the range from 1.3 to 2.[30] Therefore, the epi-CdS/epi-CdTe device with A of 1.79 shows a better device performance. The A of 1.79 also indicates the current is controlled by trap recombination in the space−charge region of the CdTe layer, whereas, for A (3.62) > 2, in addition to the space−charge recombination, it indicates there is a tunneling barrier at the interface of the poly-CdS/epi-CdTe device, which increases the probability of carrier recombination at the interface.[33,34] This speculation is also evidenced by the higher J_0 (3.2 × 10^{-2} mA cm^{-2}) of the poly-CdS/epi-CdTe device.

It is known that interface defects play an important role in the interface recombination of the devices. Therefore, interface defect densities of the two devices were characterized using $C-V$ profiling and DLCP.[35,36] In general, $C-V$ profiling measurement is derived by a direct-current (DC) voltage, while the DLCP measurement is derived using a small alternating current (AC) at different bias voltages. The defect density extracted from the $C-V$ profiling (N_{CV}) includes the response of free carriers, and bulk and interface defects, whereas the defect density from DLCP (N_{DLCP}) represents the response only from free carriers and bulk defects.[36] Then the interface defect density can be extracted from the difference between N_{CV} and N_{DLCP}. The data analysis details of $C-V$ profiling and DLCP are provided in Supporting Information section 3. Figure 6f shows the plots of N_{CV} and N_{DLCP} against the depletion width (x). It can be clearly seen from Figure 6f that the difference between N_{CV} and N_{DLCP} of the poly-CdS/epi-CdTe device is much higher than that of the epi-CdS/epi-CdTe device, suggesting lower defect density and recombination loss at the epi-CdS/epi-CdTe interface. Here, the depletion widths of the poly-CdS/epi-CdTe and epi-CdS/epi-CdTe devices are 396 and 945 nm, respectively. The volume to surface ratio is the depletion width. The interface defect densities of the poly-CdS/epi-CdTe and epi-CdS/epi-CdTe devices can be calculated to be 8.2 × 10^{10} and 6.8 × 10^{10} cm^{-2} (Table 2), respectively. Consequently, we conclude that the interface defects of CdS/CdTe solar cells can be reduced by employing both epitaxial CdS and CdTe films.

The junction photoluminescence characterization was used to further investigate the interface property of poly-CdS/epi-CdTe and epi-CdS/epi-CdTe devices. Figure S5a shows the PL spectra of the two devices. The PL measurements were carried out with excitation from the CdS side, as illustrated in the inset of Figure S5a. The laser (405 nm) can go through the CdS layer and excite the interface of CdS/CdTe heterojunction. Two PL peaks were observed from the poly-CdS/epi-CdTe device at the positions of 509 and 821 nm. Three PL peaks were observed from the epi-CdS/epi-CdTe device at the positions of 513, 701, and 828 nm. The PL emissions around 510 nm are from the intrinsic CdS layer.[37,38] The PL emissions at 821 and 828 nm are from the CdTe layer.[39] The broad PL peak at 701 nm was excited from the mixed CdS_xTe_{1-x},[39] which formed during the deposition of CdTe layer at the substrate temperature of 420 °C, whereas, for the poly-CdS/epi-CdTe device, the CdS layer was deposited on epi-CdTe at room temperature. There is no CdS_xTe_{1-x} layer formed at the interface of the poly-CdS/epi-CdTe heterojunction. The formation of CdS_xTe_{1-x} mixed crystal layer reduced the interface defects at the epi-CdS/epi-CdTe heterojunction.[40] The result is consistent with the $C-V$ profiling and DLCP results that the epi-CdS/epi-CdTe device has lower interface defects. In addition, the formation of CdS_xTe_{1-x} mixed layer can reduce the thickness of the CdS layer, which enables more light going through the CdS layer and incident into the absorb layer. That is one possible reason why the epi-CdS/epi-CdTe device has a stronger photoresponse in the range of 300−500 nm (Figure 6d). The time-resolved PL (TRPL) decay curves

https://dx.doi.org/10.1021/acsaem.0c00265
ACS Appl. Energy Mater. 2020, 3, 4589−4599

of the PL peaks are shown in Figure S5b,c. The PL lifetimes could be fitted using the following bi-exponential mode:

$$A(t) = A_1 \exp(-t/\tau_1) + A_2 \exp(-t/\tau_2) \quad (3)$$

where $A(t)$ is the PL intensity at the time of t and A_1 and A_2 are the amplitudes of components with lifetimes of τ_1 and τ_2, respectively. The PL lifetime consists of a short lifetime τ_1 dominated by carrier drift and diffusion, and a long lifetime τ_2 probably limited by Shockley−Read−Hall recombination of carriers.[39] The fitting results are given in Figure S5b,c. Compared to the poly-CdS/epi-CdTe device, the epi-CdS/epi-CdTe device shows longer PL lifetimes (for 828 nm, τ_1 for 0.18 ns vs 0.10 ns and τ_2 for 3.53 ns vs 1.34 ns; for 514 nm, τ_1 for 49 ps vs 31 ps and τ_2 for 321 ps vs 225 ps, respectively), which indicates that the epi-CdS/epi-CdTe device has a better interface with a lower carrier recombination. The PL decay from the epi-CdTe exhibited a longer lifetime (3.53 ns) than that of the reported polycrystalline CdTe (3.0 ns),[41] indicating a higher quality of the epi-CdTe film. For the 701 nm PL emission from the CdS_xTe_{1-x} mixed layer of epi-CdS/epi-CdTe device, the short lifetime τ_1 is 1.09 ns and the long lifetime τ_2 is 8.58 ns. These longer lifetimes demonstrate that the CdS_xTe_{1-x} mixed layer passivated the epi-CdS/epi-CdTe heterointerface and reduced the interface defects and the carrier recombination.

For the poly-CdS/epi-CdTe device, the CdS buffer layer was thermally evaporated on epi-CdTe/Cu/Au/SU-8 at room temperature. No annealing was employed on the device during and after the fabrication process to improve the junction quality due to the instability of SU-8 at an elevated annealing temperature, whereas the epi-CdTe film was grown on epi-CdS/mica at the substrate temperature of 420 °C, which resulted in a higher quality CdS/CdTe interface. It can be confirmed by the lower ideality factor of the junction (Figure 6e) and interface defect density (Figure 6f and Table 2). These superior properties of the epi-CdS/epi-CdTe junction contribute to the higher efficiency. Generally, after ITO deposition, the devices should be annealed at the temperature above 200 °C to improve the front contact of ITO electrodes.[6] But there was no postannealing employed for our devices, because cracks and damages would form in the SU-8 substrate when annealed at the temperature above 200 °C. If the substrate permits postannealing for the devices to improve the front contact of ITO/CdS, higher fill factor and efficiency will be achieved. That is why only 54.3% fill factor was obtained for our epi-CdS/epi-CdTe flexible solar cells. It should be noted that the flexible substrate is crucially important to the performance of flexible solar cells. As mentioned before, the flexible CdTe solar cells with superstrate structure fabricated on polyimide (PI) film had an efficiency of 13.8%.[1] The substrate structured flexible device fabricated on metal foil showed an efficiency of 13.6%.[6] With the willow glass as substrate, CdS:O instead of CdS buffer layer and ZnTe:Cu/Au as the back-contact layers, the efficiency of superstrate flexible CdTe solar cells had been improved to 16.4%.[5] Through this work, the fabrication of flexible CdTe solar cells with the transferred epitaxial films demonstrates a great potential of epitaxial films in flexible electronic devices applications.

4. CONCLUSION

In summary, we have demonstrated the epitaxy growth of CdTe thin films on mica substrates by vapor transport deposition process. The high quality of epitaxial CdTe films were confirmed by XRD and EBSD characterizations. The epitaxial films have been successfully separated from mica through the surface tension of water and transferred to other substrate without any noticeable damage formed. This process is based on the weak interaction at the interface of epitaxial film and substrate. The transfer method can be applied to other epitaxial films grown on weakly interacting substrates. All-epitaxial, flexible CdS/CdTe solar cells with an efficiency of 9.59% were fabricated through the transfer method. It is found that the all-epitaxial CdS/CdTe solar cells possess lower interface defects, longer PL lifetime, and higher diode quality than that of the poly-CdS/epi-CdTe solar cells. These encouraging results highlight the potential of epitaxial films to be used for flexible electronic devices.

■ ASSOCIATED CONTENT

Supporting Information

The Supporting Information is available free of charge at https://pubs.acs.org/doi/10.1021/acsaem.0c00265.

XRD characterization; Raman spectra; $J-V$ curves; normalized PCE as a function of bending angle; PL characterization; device performance parameters; details of $C-V$ profiling and DLCP analysis (PDF)

■ AUTHOR INFORMATION

Corresponding Author

Xixing Wen − *Center for Materials, Devices and Integrated Systems and Department of Physics, Applied Physics and Astronomy, Rensselaer Polytechnic Institute, Troy, New York 12180, United States;* orcid.org/0000-0003-2593-8612; Email: wenx3@rpi.edu

Authors

Zonghuan Lu − *Center for Materials, Devices and Integrated Systems and Department of Physics, Applied Physics and Astronomy, Rensselaer Polytechnic Institute, Troy, New York 12180, United States;* orcid.org/0000-0003-2375-8247

Xin Sun − *Center for Materials, Devices and Integrated Systems and Department of Physics, Applied Physics and Astronomy, Rensselaer Polytechnic Institute, Troy, New York 12180, United States*

Yu Xiang − *Center for Materials, Devices and Integrated Systems and Department of Physics, Applied Physics and Astronomy, Rensselaer Polytechnic Institute, Troy, New York 12180, United States*

Zhizhong Chen − *Center for Materials, Devices and Integrated Systems and Department of Materials Science and Engineering, Rensselaer Polytechnic Institute, Troy, New York 12180, United States*

Jian Shi − *Center for Materials, Devices and Integrated Systems and Department of Materials Science and Engineering, Rensselaer Polytechnic Institute, Troy, New York 12180, United States;* orcid.org/0000-0003-2115-2225

Ishwara Bhat − *Center for Materials, Devices and Integrated Systems and Department of Electrical, Computer and Systems Engineering, Rensselaer Polytechnic Institute, Troy, New York 12180, United States*

Gwo-Ching Wang − *Center for Materials, Devices and Integrated Systems and Department of Physics, Applied Physics and Astronomy, Rensselaer Polytechnic Institute, Troy, New York 12180, United States*

https://dx.doi.org/10.1021/acsaem.0c00265
ACS Appl. Energy Mater. 2020, 3, 4589−4599

Morris Washington − *Center for Materials, Devices and Integrated Systems and Department of Physics, Applied Physics and Astronomy, Rensselaer Polytechnic Institute, Troy, New York 12180, United States*

Toh-Ming Lu − *Center for Materials, Devices and Integrated Systems and Department of Physics, Applied Physics and Astronomy, Rensselaer Polytechnic Institute, Troy, New York 12180, United States*

Complete contact information is available at: https://pubs.acs.org/10.1021/acsaem.0c00265

Notes

The authors declare no competing financial interest.

■ ACKNOWLEDGMENTS

This work was supported by the Empire State Development's Division of Science, Technology and Innovation (NYSTAR) through Focus Center—New York Contract C150117 and Rensselaer. Z.C. and J. S. were supported by the National Science Foundation under Award No. 1706815. We acknowledge MNCR staff at RPI for, in part, facilitating the experimental work.

■ REFERENCES

(1) Kranz, L.; Buecheler, S.; Tiwari, A. N. Technological status of CdTe photovoltaics. *Sol. Energy Mater. Sol. Cells* **2013**, *119*, 278−280.

(2) Tao, M., Status of solar photovoltaics. In *Terawatt Solar Photovoltaics*, 2014th, Ed. Springer: London, 2014; pp 9−20, DOI: 10.1007/978-1-4471-5643-7_2.

(3) *NREL Best Research-Cell Efficiency Chart*; National Renewable Energy Laboratory, https://www.nrel.gov/pv/assets/pdfs/best-research-cell-efficiencies.20200311.pdf (Accessed 2020-03-11).

(4) Ramanujam, J.; Bishop, D. M.; Todorov, T. K.; Gunawan, O.; Rath, J.; Nekovei, R.; Artegiani, E.; Romeo, A. Flexible CIGS, CdTe and a-Si: H based thin film solar cells: A review. *Prog. Mater. Sci.* **2020**, *110*, 100619.

(5) Mahabaduge, H. P.; Rance, W. L.; Burst, J. M.; Reese, M. O.; Meysing, D. M.; Wolden, C. A.; Li, J.; Beach, J. D.; Gessert, T. A.; Metzger, W. K.; Garner, S.; Barnes, T. M. High-efficiency, flexible CdTe solar cells on ultra-thin glass substrates. *Appl. Phys. Lett.* **2015**, *106*, 133501.

(6) Kranz, L.; Gretener, C.; Perrenoud, J.; Schmitt, R.; Pianezzi, F.; La Mattina, F.; Blosch, P.; Cheah, E.; Chirila, A.; Fella, C. M.; Hagendorfer, H.; Jager, T.; Nishiwaki, S.; Uhl, A. R.; Buecheler, S.; Tiwari, A. N. Doping of polycrystalline CdTe for high-efficiency solar cells on flexible metal foil. *Nat. Commun.* **2013**, *4*, 2306.

(7) Zhao, Y.; Boccard, M.; Liu, S.; Becker, J.; Zhao, X. H.; Campbell, C. M.; Suarez, E.; Lassise, M. B.; Holman, Z.; Zhang, Y. H. Monocrystalline CdTe solar cells with open-circuit voltage over 1V and efficiency of 17%. *Nat. Energy* **2016**, *1*, 16067.

(8) Liu, S.-C.; Yang, Y.; Li, Z.; Xue, D.-J.; Hu, J.-S. GeSe thin-film solar cells. *Mater.Chem.Front.* **2020**, *4*, 775−787.

(9) Koma, A. Van der Waals epitaxy-a new epitaxial growth method for a highly lattice-mismatched system. *Thin Solid Films* **1992**, *216*, 72−76.

(10) Mohanty, D.; Lu, Z. H.; Sun, X.; Xiang, Y.; Wang, Y. P.; Ghoshal, D.; Shi, J.; Gao, L.; Shi, S. S.; Washington, M.; Wang, G.-C.; Lu, T.-M.; Bhat, I. Metalorganic vapor phase epitaxy of large size CdTe grains on mica through chemical and van der Waals interactions. *Phys. Rev. Mater.* **2018**, *2*, 113402.

(11) Wang, Y. P.; Gao, L.; Yang, Y. B.; Xiang, Y.; Chen, Z. Z.; Dong, Y. Q.; Zhou, H.; Cai, Z. H.; Wang, G.-C.; Shi, J. Nontrivial strength of van der Waals epitaxial interaction in soft perovskites. *Phys. Rev. Mater.* **2018**, *2*, No. 076002.

(12) Lian, Q.; Zhu, X. T.; Wang, X. D.; Bai, W.; Yang, J.; Zhang, Y. Y.; Qi, R. J.; Huang, R.; Hu, W. D.; Tang, X. D.; Wang, J. L.; Chu, J. H. Ultrahigh-Detectivity Photodetectors with Van der Waals Epitaxial CdTe Single-Crystalline Films. *Small* **2019**, *15*, 1900236.

(13) Yang, Y.; Seewald, L.; Mohanty, D.; Wang, Y.; Zhang, L.; Kisslinger, K.; Xie, W.; Shi, J.; Bhat, I.; Zhang, S.; Lu, T.-M.; Wang, G.-C. Surface and interface of epitaxial CdTe film on CdS buffered van der Waals mica substrate. *Appl. Surf. Sci.* **2017**, *413*, 219−232.

(14) Cheng, R. Q.; Wen, Y.; Yin, L.; Wang, F. M.; Wang, F.; Liu, K. L.; Shifa, T. A.; Li, J.; Jiang, C.; Wang, Z. X.; He, J. Ultrathin Single-Crystalline CdTe Nanosheets Realized via Van der Waals Epitaxy. *Adv. Mater.* **2017**, *29*, 1703122.

(15) Mohanty, D.; Lu, Z. H.; Sun, X.; Xiang, Y.; Gao, L.; Shi, J.; Zhang, L. H.; Kisslinger, K.; Washington, M. A.; Wang, G.-C.; Lu, T.-M.; Bhat, I. B. Growth of epitaxial CdTe thin films on amorphous substrates using single crystal graphene buffer. *Carbon* **2019**, *144*, 519−524.

(16) Neretina, S.; Hughes, R.; Sochinskii, N.; Weber, M.; Lynn, K.; Wojcik, J.; Pearson, G.; Preston, J.; Mascher, P. Growth of CdTe/Si(100) thin films by pulsed laser deposition for photonic applications. *J. Vac. Sci. Technol., A* **2006**, *24*, 606−611.

(17) Lischka, K.; Fantner, E.; Ryan, T.; Sitter, H. J. A. P. L. X-ray rocking curves from (100) and (111)CdTe grown on (100)GaAs by hot wall epitaxy. *Appl. Phys. Lett.* **1989**, *55*, 1309−1311.

(18) Escobedo, A.; Quinones, S.; Adame, M.; McClure, J.; Zubia, D.; Brill, G. Characterization of Smooth CdTe(111) Films by the Conventional Close-Spaced Sublimation Technique. *J. Electron. Mater.* **2010**, *39*, 400−409.

(19) Kim, T.; Jung, M.; Park, H.; Na, H.; Kim, J. Interdiffusion problems at CdTe/InSb heterointerfaces grown by temperature gradient vapor transport deposition. *Appl. Phys. Lett.* **1992**, *61*, 1101−1103.

(20) Kim, T.; Koo, B.; Jung, M.; Kim, S.; Park, H.; Lim, H.; Lee, J.; Kang, K. Growth of CdTe epitaxial films on p-InSb(111) by temperature gradient vapor transport deposition. *J. Appl. Phys.* **1992**, *71*, 1049−1051.

(21) Kestner, J. M.; McElvain, S.; Kelly, S.; Ohno, T. R.; Woods, L. M.; Wolden, C. A. An experimental and modeling analysis of vapor transport deposition of cadmium telluride. *Sol. Energy Mater. Sol. Cells* **2004**, *83*, 55−65.

(22) Amirtharaj, P.; Pollak, F. H. Raman scattering study of the properties and removal of excess Te on CdTe surfaces. *Appl. Phys. Lett.* **1984**, *45*, 789−791.

(23) Jung, Y.; Yang, G.; Chun, S.; Kim, D.; Kim, J. Growth of CdTe thin films on graphene by close-spaced sublimation method. *Appl. Phys. Lett.* **2013**, *103*, 231910.

(24) Sun, X.; Wang, Y. P.; Seewald, L. J.; Chen, Z. Z.; Shi, J.; Washington, M. A.; Lu, T.-M. Decoupling interface effect on the phase stability of CdS thin films by van der Waals heteroepitaxy. *Appl. Phys. Lett.* **2017**, *110*, No. 041602.

(25) Sun, X.; Lu, Z. H.; Xie, W. Y.; Wang, Y. P.; Shi, J.; Zhang, S. B.; Washington, M. A.; Lu, T.-M. van der Waals epitaxy of CdS thin films on single-crystalline graphene. *Appl. Phys. Lett.* **2017**, *110*, 153104.

(26) Rance, W. L.; Burst, J. M.; Meysing, D. M.; Wolden, C. A.; Reese, M. O.; Gessert, T. A.; Metzger, W. K.; Garner, S.; Cimo, P.; Barnes, T. M. 14%-efficient flexible CdTe solar cells on ultra-thin glass substrates. *Appl. Phys. Lett.* **2014**, *104*, 143903.

(27) Lin, X. Z.; Klenk, R.; Wang, L.; Kohler, T.; Albert, J.; Fiechter, S.; Ennaoui, A.; Lux-Steiner, M. C. 11.3% efficiency $Cu(In,Ga)(S,Se)_2$ thin film solar cells via drop-on-demand inkjet printing. *Energy Environ. Sci.* **2016**, *9*, 2037−2043.

(28) Sites, J.; Mauk, P. Diode quality factor determination for thin-film solar cells. *Sol. Cells* **1989**, *27*, 411−417.

(29) Sites, J. Quantification of losses in thin-film polycrystalline solar cells. *Sol. Energy Mater. Sol. Cells* **2003**, *75*, 243−251.

(30) Hegedus, S. S.; Shafarman, W. Thin-film solar cells: device measurements and analysis. *Prog. Photovoltaics* **2004**, *12*, 155−176.

(31) Wen, X.; He, Y.; Chen, C.; Liu, X.; wang, L.; Yang, B.; Leng, M.; Song, H.; Zeng, K.; Li, D.; Li, K.; Gao, L.; Tang, J. Magnetron sputtered ZnO buffer layer for Sb_2Se_3 thin film solar cells. *Sol. Energy Mater. Sol. Cells* **2017**, *172*, 74−81.

(32) Wang, L.; Luo, M.; Qin, S.; Liu, X.; Chen, J.; Yang, B.; Leng, M.; Xue, D.-J.; Zhou, Y.; Gao, L.; Song, H.; Tang, J. Ambient $CdCl_2$ treatment on CdS buffer layer for improved performance of Sb_2Se_3 thin film photovoltaics. *Appl. Phys. Lett.* **2015**, *107*, 143902.
(33) Bayhan, H.; Kavasoğlu, A. S. Tunnelling enhanced recombination in polycrystalline CdS/CdTe and CdS/Cu(In,Ga)Se_2 heterojunction solar cells. *Solid-State Electron.* **2005**, *49*, 991−996.
(34) Echendu, O.; Fauzi, F.; Weerasinghe, A.; Dharmadasa, I. High short-circuit current density CdTe solar cells using all-electrodeposited semiconductors. *Thin Solid Films* **2014**, *556*, 529−534.
(35) Heath, J. T.; Cohen, J. D.; Shafarman, W. Bulk and metastable defects in $CuIn_{1-x}Ga_xSe_2$ thin films using drive-level capacitance profiling. *J. Appl. Phys.* **2004**, *95*, 1000−1010.
(36) Duan, H. S.; Yang, W.; Bob, B.; Hsu, C. J.; Lei, B.; Yang, Y. The role of sulfur in solution-processed $Cu_2ZnSn(S,Se)_4$ and its effect on defect properties. *Adv. Funct. Mater.* **2013**, *23*, 1466−1471.
(37) Liu, B.; Chen, R.; Xu, X. L.; Li, D. H.; Zhao, Y. Y.; Shen, Z. X.; Xiong, Q. H.; Sun, H. D. Exciton-Related Photoluminescence and Lasing in CdS Nanobelts. *J. Phys. Chem. C* **2011**, *115*, 12826−12830.
(38) Lozada-Morales, R.; Zelaya-Angel, O.; Torres-Delgado, G. Photoluminescence in cubic and hexagonal CdS films. *Appl. Surf. Sci.* **2001**, *175−176*, 562−566.
(39) Kuciauskas, D.; Kanevce, A.; Duenow, J. N.; Dippo, P.; Young, M.; Li, J. V.; Levi, D. H.; Gessert, T. A. Spectrally and time resolved photoluminescence analysis of the CdS/CdTe interface in thin-film photovoltaic solar cells. *Appl. Phys. Lett.* **2013**, *102*, 173902.
(40) Okamoto, T.; Murata, A.; Hayashi, Y.; Watanabe, D.; Araki, H.; Katagiri, H. Effects of Cu doping on CdTe thin-film solar cells in substrate configuration. *Jpn. J. Appl. Phys.* **2019**, *58*, SBBF08.
(41) Li, D. B.; Song, Z. N.; Awni, R. A.; Bista, S. S.; Shrestha, N.; Grice, C. R.; Chen, L.; Liyanage, G. K.; Razooqi, M. A.; Phillips, A. B.; Heben, M. J.; Ellingson, R. J.; Yan, Y. F. Eliminating S-Kink To Maximize the Performance of MgZnO/CdTe Solar Cells. *ACS Appl. Energy mater.* **2019**, *2*, 2896−2903.

https://dx.doi.org/10.1021/acsaem.0c00265
ACS Appl. Energy Mater. 2020, 3, 4589−4599